FEEDBACK LINEARIZATION IN A SIX DEGREE-OF-FREEDOM MAG-LEV STAGE

Stephen J. Ludwick
Department of Mechanical Engineering
Massachusetts Institute of Technology
Cambridge, Massachusetts

David L. Trumper
Department of Mechanical Engineering
Massachusetts Institute of Technology
Cambridge, Massachusetts

Michael L. Holmes
Department of Electrical Engineering
University of North Carolina at Charlotte
Charlotte, North Carolina

ABSTRACT

A six degree–of–freedom electromagnetically suspended motion control stage (the Angstrom Stage) has been designed and constructed for use in short-travel, high-resolution motion control applications. It achieves better than 0.5 nm resolution over a 100 micron range of travel. The stage consists of a single moving element (the platen) floating in an oil filled chamber. The oil is crucial to the stage's operation since it forms squeeze film dampers between the platen and the frame. Twelve electromagnetic actuators provide the forces necessary to suspend and servo the platen, and six capacitance probes measure its position relative to the frame. The system is controlled using a digital signal processing board residing in a '486 based PC. This digital controller implements a feedback linearization algorithm in real-time to account for nonlinearities in both the magnetic actuators and the fluid film dampers. The feedback linearization technique reduces a highly nonlinear plant with coupling between the degrees of freedom into one that is linear, decoupled, and setpoint independent. The key to this procedure is a detailed plant model. The operation of the feedback linearization procedure is transparent to the outer loop of the controller, and so a proportional controller is sufficient for normal operation. We envision applications of this stage in scanned probe microscopy and for integrated circuit measurement.

INTRODUCTION

The Angstrom Stage is a motion control device that utilizes electromagnetic actuators in combination with squeeze film dampers to achieve sub-nanometer resolution with travel in a cube of 100 microns. Details concerning the mechanical design of the stage are found in [1]. In addition, [2] gives examples of atomic resolution images that were generated when the stage was paired with a scanning tunneling microscope. Rather than emphasizing the mechanical design of the stage, this paper instead concentrates on the feedback linearization algorithm that is key to the controller design. Using a model of the plant, this algorithm linearizes and decouples the six degrees of freedom. Linearizing the electromagnetic actuators with this technique is a standard procedure in our group's design process [3] [4] [5] [6]. In this paper, we expand the technique to include reducing the plant itself to six decoupled integrators with transfer functions of $1/s$ each. Hunt [7] and Su [8] provide a more general, mathematically rigorous description of the feedback linearization procedure.

MECHANICAL DESIGN AND MODELING

The Angstrom Stage consists of a platen floating in an oil–filled[1] chamber formed by an outer frame. Figure 1 shows a photograph of the device seated on a tabletop vibration isolation table. This frame has exterior dimensions of approximately $30 \times 30 \times 20$ cm, and is constructed from 6061-T6 aluminum. The platen is also made from aluminum, measures $17 \times 17 \times 8$ cm, and is designed with a hollow interior. This lightweighting of the platen is designed so that the platen's mass approximately equals the mass of the fluid it displaces. In practice, the oil supports better than 98% of the 3.09 kg mass of the platen. This reduces the bias currents required to keep the platen suspended, and thus reduces the associated thermal distortions of the frame. However, the most important function of the oil is the forming of squeeze film dampers between the platen and the frame. This will be described in more detail later in the paper. The end result is a highly overdamped and vibration resistant design. A cross section and an isometric view of the stage are shown in Figure 2.

Electromagnetic Actuators

Twelve electromagnetic actuators provide the forces necessary to suspend and servo the platen. Each actuator is fabricated with 230 turns of 22 gauge copper wire around 50-50 Ni-Fe E–Core laminations. The actuators are potted directly into the frame and act upon corresponding 50-50 Ni-Fe I–laminations epoxied into the platen. The actuators are

---

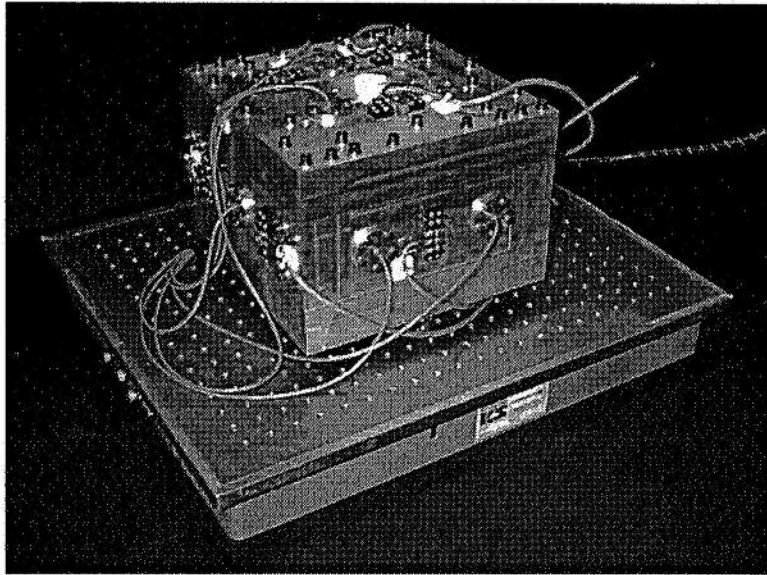[1]Dow Corning FS-1265 fluorosilicone oil, density $= 1.28$ g/cm^3, viscosity $= 1.323$ kg/ms

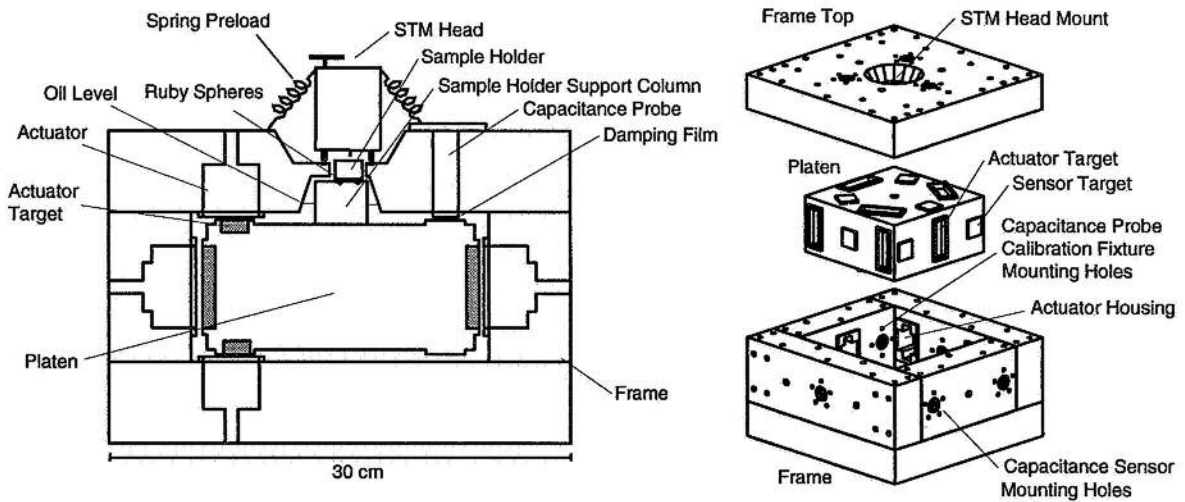Figure 1: Photograph of the Angstrom Stage.

Figure 2: Angstrom Stage Cross Section and Isometric View.

97

designed to operate at a nominal gap of 300 μm, and are capable of producing over 50 N of force at this gap. However, normal operating forces are less than 1 N. The relationship between force, current, and gap is nonlinear, and is well modeled in the low–current region by

$$F\left(i, g_a\right) = C\left(\frac{i}{g_a}\right)^2.$$ (1)

Low currents are those for which the electromagnet has not begun to enter saturation, i.e., less than about 1 A in this application. In eq.(1), F represents the electromagnetic force, i is the coil current, and g_a is the target separation gap. The constant C is experimentally determined with our magnetic bearing calibration fixture [9], and equals approximately 2.5×10^{-6} Nm^2/A^2 for this design.

Squeeze Film Dampers

The dominant components of the stage, with respect to the system dynamics, are the squeeze film dampers formed by the thin film of oil located between the platen and the actuators and capacitance probes. The relationship between force and velocity at each capacitance probe comes from a direct application of the Navier–Stokes equation for viscous fluid flow [10],

$$F = \frac{3\pi\mu R^4}{2g_c^3}V.$$ (2)

The key fact to note here is that the damping changes with the inverse cube of the gap. The oil viscosity ($\mu = 1.323$ kg/ms), and the capacitance probe radius ($R = 0.01$ m) combine into a single characteristic constant b_c for the capacitance probe dampers. This reduces the force–velocity relationship to

$$F = \frac{b_c}{g_c^3}V,$$ (3)

where $b_c = 6.2 \times 10^{-8}$ Nsm^2. At the nominal oil film thickness of $g_c = 100$ μm, each probe contributes a damping term of $B_c = 6.2 \times 10^4$ Ns/m. However, this value changes significantly over the ± 50 μm range of travel due to the g_c^{-3} dependence.

The relationship between force and velocity for the actuator dampers is more difficult to model in a closed form because of their rectangular shape. It instead results in an infinite series solution [11],

$$F = \frac{192\mu l^3 V}{\pi^4 g_a^3} \sum_{n=1,3,5}^{\infty} \left(\frac{b}{2n^4} - \frac{l}{n^5\pi}\tanh\frac{n\pi b}{2l}\right).$$ (4)

The summation contains only the known width ($b = 0.06$ m) and length ($l = 0.025$ m) of the damping pad, and so evaluates to a constant independent of the gap. Thus the
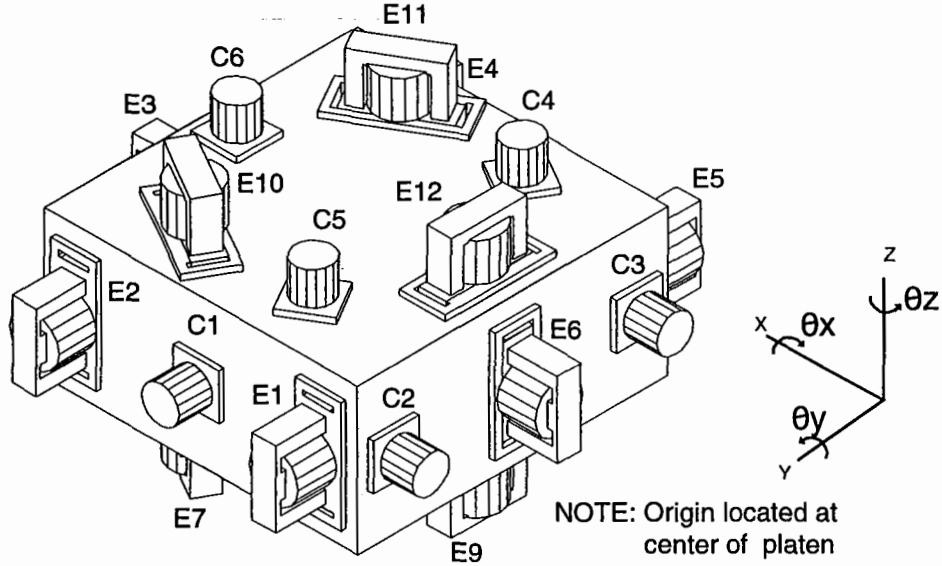
Figure 3: Location of Probes and Actuators Relative to the Platen.

damping due to an actuator in our system can be expressed as

$$F = \frac{b_a}{g_a^3} V, \tag{5}$$

with $b_a = 9.1 \times 10^{-7}$ Nsm^2. At the nominal oil film thickness of $g_a = 300$ μm, each actuator then contributes a damping term to the system of $B_a = 3.4 \times 10^4$ Ns/m. Again though, this factor changes significantly as the platen moves.

Equations (2) and (4) give the damping values for a single probe and actuator. In the stage operation, multiple dampers act on the platen with every motion. Figure 3 shows the the positions of the actuators and capacitance probes relative to the platen. It now becomes easier to express the force–velocity relationship in a matrix format,

$$\mathbf{F} = \mathbf{BV}. \tag{6}$$

The forces (and torques) $\mathbf{F}$ and velocities $\mathbf{V}$ are defined as

$$\mathbf{F} = \begin{bmatrix} F_x & F_y & F_z & T_x & T_y & T_z \end{bmatrix}^T, \tag{7}$$

and

$$\mathbf{V} = \begin{bmatrix} \dot{x} & \dot{y} & \dot{z} & \dot{\theta}_x & \dot{\theta}_y & \dot{\theta}_z \end{bmatrix}^T. \tag{8}$$

The 6×6 damping matrix $\mathbf{B}$ is an instantaneous function of the stage position, and couples motions in the different axes. Its components are algebraically complex even though it is derived simply from free body diagrams of the platen motion. These relationships are given in the Appendix. For perspective on the magnitude of the damping values in the combined model, Figures 4 and 5 shows the damping in each degree of freedom as the stage moves from plus to minus full scale in that axis.
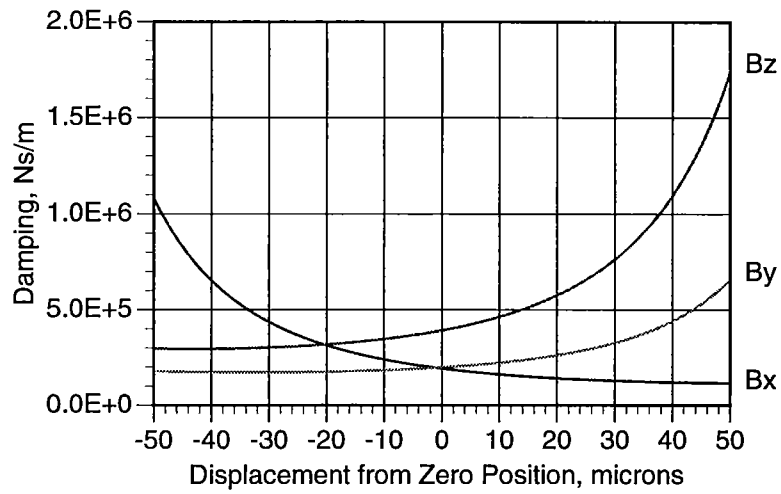
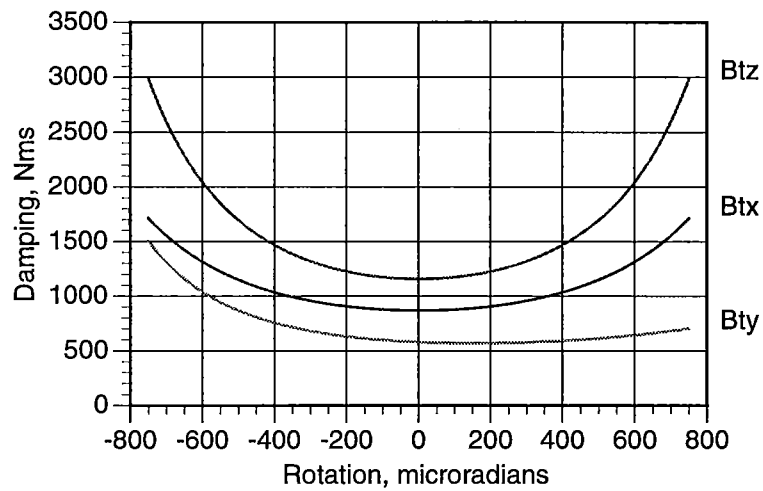Figure 4: Damping Coefficients as the Stage Moves in the Translational Directions.

Figure 5: Damping Coefficients as the Stage Moves in the Rotational Directions.

CONTROLLER

A digital computer controls the operation of the Angstrom Stage. A 16-bit analog–to–digital conversion board reads the six capacitance probe voltages (as well as a Z-servo voltage from a scanning tunneling microscope) into a '486-based PC . Each channel is sampled at 22.3 kHz, which brings the overall sampling rate for the board close to the board's maximum throughput of 160 ksamples/second. A TMS320C30–based digital signal processing board implements a 100 point finite impulse response filter in order to increase the position resolution and lessen the noise magnitude. Finite processor speed requires that the resulting waveform be downsampled by thirty points before the remainder of the controller operates on filtered position measurements. This reduces the controller update rate to about 744 Hz. The C30 performs the control calculations and writes the required voltages to a 12-bit digital–to–analog converter board. Finally, twelve linear transconductance power amplifiers transduce these voltages into actuator currents.

The controller design begins with a model of the stage. In this case, the fluid film dampers dominate the dynamics to the point where the stage can be modeled as a pure integrator. The velocity along any axis is thus simply proportional to the force applied by the electromagnetic actuators along that axis. However, the applied force is a nonlinear function of the gaps and the current, and the damping is also a nonlinear function of the gaps. Closing the loop with a typical Proportional (P) or Proportional-Integral (PI) controller will stabilize the plant. However, the response to a commanded change in position will depend upon where the platen is located. Also, a typical controller will not lead to constant velocity motion as is required in a scanning stage.

As an alternative, we approach the design with a set of desired velocities in each of the six directions (three translational and three rotational). The controller utilizes a model of the plant,

$$\mathbf{F}_d = \widehat{\mathbf{B}} \mathbf{V}_d, \tag{9}$$

that calculates the forces and torques that will produce these target velocities. The plant model is derived by calculating the damping coefficients for each of the fluid film dampers, and relating these to the cartesian axes. Off–diagonal terms in the $\widehat{\mathbf{B}}$ matrix indicate the inherent coupling between the axes. Its component elements are calculated in real–time by the digital signal processor on the basis of the damping models presented earlier.

The second step of the feedback linearization is to determine what currents should be applied in order to generate the desired forces. This is accomplished by inverting the actuator dynamics, leading to

$$i = \hat{g}_a \sqrt{\frac{F_d}{\widehat{C}}}. \tag{10}$$

If the estimates of the gaps, force constants, and damping factors are accurate, the velocity of the plant will match the reference velocity. At this point, the controller can use the linearized plant in two ways. One is to simply command constant velocities in order to generate a scanning motion. The accuracy of the model determines the performance of this
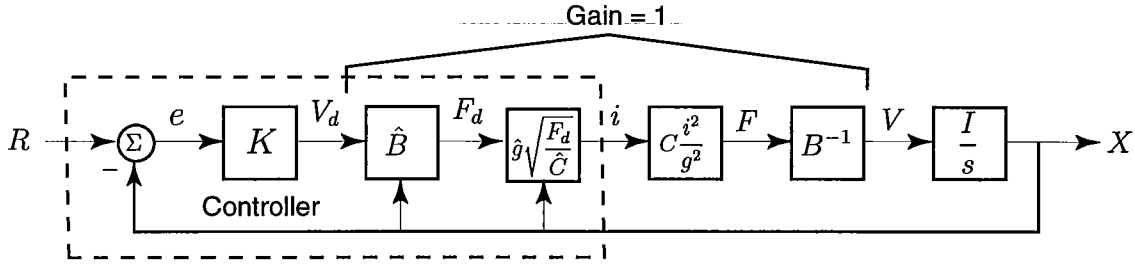
Figure 6: Block Diagram of Feedback Linearization Scheme.

open loop velocity controller. More typically, we can feed back the position readings in a PI control scheme. In this case, the operation of the linearization component of the controller is transparent. The main outer loop can simply be designed to control a decoupled plant with transfer functions of $1/s$ in each of six degrees of freedom. This control mode is useful for small displacements and maintaining stability about a setpoint. The block diagram of this feedback control scheme is shown in Figure 6.

RESULTS

As was stated in the previous section, the stage operates in both an open loop velocity control mode and in a closed loop position control mode. The velocity control is important for providing motion in the fast direction of a scanning pattern. Using closed loop position control in this case would result in an exponential approach to a target position, and therefore a non-uniform velocity. However, closed loop control on the position in the slow scan direction allows the stage to move a set distance for each new scan. Maintaining position stability in that axis ensures that the repeated scans lie parallel to each other. The magnitude of the position error determines in which control mode the stage is operating. Large position errors cause the stage to move with a constant velocity while small errors are handled by closed loop position control.

Experimental data from the open loop constant velocity control mode is shown in Figure 7. This figure illustrates the accuracy of the plant model and the effectiveness of the open loop velocity control. The stage moves with a commanded velocity of -2 μm/s from a position at $x = +25$ μm to one at $x = -20$ μm. Over that span, the damping coefficient in the x-direction increases over 2.7 times from 135,300 Ns/m to 369,200 Ns/m. Figure 8 contains a plot of the error between the data in Figure 7 and the best–fit line. The maximum error at any time is less than 20 nm, but more importantly, the error follows a repeatable pattern. This shape is due to manufacturing errors which changed the null actuator and capacitance probe gaps from their nominal values of 300 μm and 100 μm respectively. By fitting responses such as these to the plant models, we were able to generate better estimates of the true gaps. Figure 8 shows both the success of this approach, and that there is still room to improve the model. In the future we plan to add
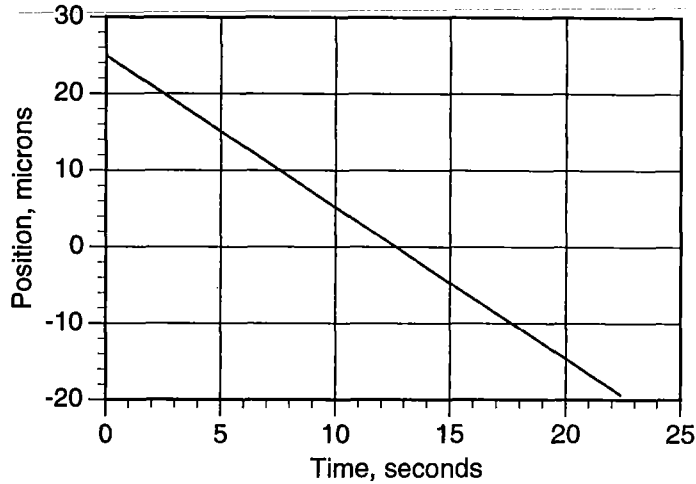
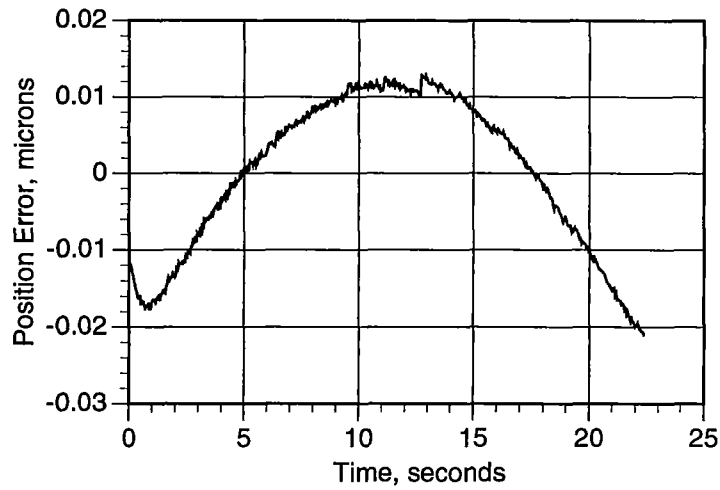Figure 7: Examples of a constant velocity scan.

Figure 8: Error in a constant velocity scan.

closed loop velocity control to the plant. To date, this has not been implemented simply because processor time has been devoted to the more immediate goal of position resolution.

Once the position error in an axis is less than 100 nm, the controller switches to the closed loop position control mode for that axis. An example of multiple 0.5 nm steps is shown in Figure 9. For this measurement, the control bandwidth is set at 5 Hz, and the measurement is taken through a differential amplifier with a bandwidth of 1 Hz. In the steady stage condition, the standard deviation of the stage position (measured through a 1 Hz filter) is about 0.05 nm.
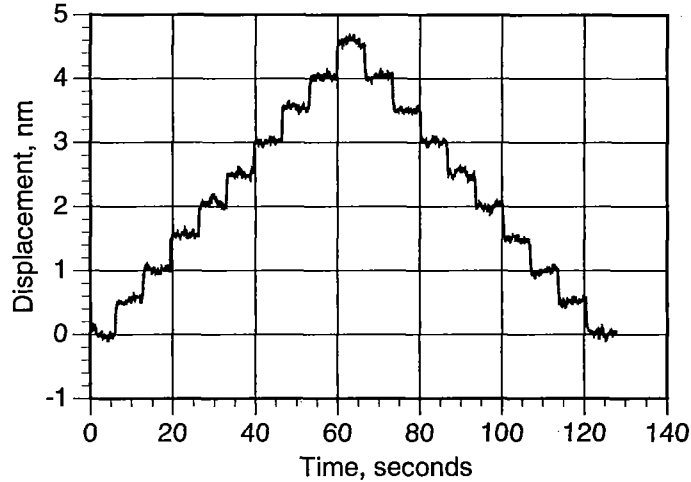
Figure 9: Repeated 0.5 nm step responses.

CONCLUSIONS

This version of the Angstrom Stage has demonstrated the feasibility of a magnetically levitated stage for use in atomic-scale motion control applications. The squeeze film dampers provide the high level of disturbance rejection necessary for a high resolution stage, but do so at the cost of a nonlinear plant with inherent coupling between the axes. The electromagnetic actuators are capable of applying precisely controlled forces, but these are again a nonlinear function of current and position. In both cases, these nonlinearities can be well modeled analytically. Including these models in a feedback linearization scheme yields a linear plant with decoupled motion in all six degrees of freedom. This stage has achieved a position noise standard deviation of 0.05 nm over a travel of 100 μm, and thus has a dynamic range of about 10^6. We believe this to be the highest-resolution magnetic suspension which has yet been constructed.

ACKNOWLEDGMENTS

BIBLIOGRAPHY

[1] M. L. Holmes: "Analysis and Design of a Magnetically Suspended Precision Motion Control Stage." M.S. Thesis, Department of Electrical Engineering, University of North Carolina at Charlotte, Charlotte, NC, 1994.

[2] M. L. Holmes; D. L. Trumper; and R. Hocken: "Atomic-Scale Precision Motion Control State (The Angstrom Stage)." *Annals of the CIRP*, 44(1):455-460, 1995.

[3] D. L. Trumper. *Magnetic Suspension Techniques for Precision Motion Control.* Ph.D. Thesis, Department of Electrical Engineering and Computer Science, Massachusetts Institute of Technology, Cambridge, MA, Sept. 1990.

[4] S. M. Alson: "Nonlinear Compensation of a Single Degree of Freedom Magnetic Suspension System." M.S. Thesis, Department of Mechanical Engineering, Massachusetts Institute of Technology, Cambridge, MA, June 1994.

[5] K. S. Chen: "A Spring-Dominated Regime Design of a High Load Capacity, Electromagnetically Driven x-y-θ stage." M.S. Thesis, Department of Mechanical Engineering, Massachusetts Institute of Technology, Cambridge, MA, June 1995.

[6] M. E. Williams; D. L. Trumper; and R. Hocken: "Magnetic Bearing Stage for Photolithography." *Annals of the CIRP*, 42(1):607-610, 1993.

[7] L. Hunt; R. Su; and G. Meyer. "Global Transformations of Nonlinear Systems." *IEEE Transactions on Automatic Control*, AC-28(1);24-30, Jan. 1983.

[8] R. Su: "On the Linear Equivalents of Nonlinear Systems." *Systems and Control Letters*, 2(1):48-52, July 1982.

[9] T. Poovey; M. L. Holmes; and D. L. Trumper: "A Kinematically Coupled Magnetic Calibration Fixture." *Precision Engineering*, 16(2), April 1994.

[10] J. A. Fay. *Introduction to Fluid Mechanics.* MIT Press, Cambridge, MA, 1994.

[11] O. Pinkus and B. Sternlicht. *Theory of Hydrodynamic Lubrication.* McGraw Hill, New York, 1961.

Damping Model

The damping model is derived simply by drawing free body diagrams of the platen with all of the nonlinear dampers around it in each degree of freedom. The six forces and torques relate to the velocities through:

$$
\begin{aligned}
F_x &= b_{xx}\dot{x} + b_{x\theta_z}\dot{\theta}_z \\
F_y &= b_{yy}\dot{y} + b_{y\theta_z}\dot{\theta}_z \\
F_z &= b_{zz}\dot{z} + b_{z\theta_x}\dot{\theta}_x + b_{z\theta_y}\dot{\theta}_y \\
T_x &= b_{\theta_x z}\dot{z} + b_{\theta_x\theta_x}\dot{\theta}_x + b_{\theta_x\theta_y}\dot{\theta}_y \\
T_y &= b_{\theta_y z}\dot{z} + b_{\theta_y\theta_x}\dot{\theta}_x + b_{\theta_y\theta_y}\dot{\theta}_y \\
T_z &= b_{\theta_z x}\dot{x} + b_{\theta_z y}\dot{y} + b_{\theta_z\theta_z}\dot{\theta}_z
\end{aligned}
$$

where the individual damping components are defined as

$$
\begin{aligned}
b_{xx} &= b_a\left(\frac{1}{g_{a3}^3} + \frac{1}{g_{a6}^3}\right) + b_c\left(\frac{1}{g_{c2}^3} + \frac{1}{g_{c3}^3}\right) \\[2mm]
b_{x\theta_z} &= b_c\ell\left(\frac{1}{g_{c3}^3} - \frac{1}{g_{c2}^3}\right) \\[2mm]
b_{yy} &= b_a\left(\frac{1}{g_{a1}^3} + \frac{1}{g_{a2}^3} + \frac{1}{g_{a4}^3} + \frac{1}{g_{a5}^3}\right) + b_c\left(\frac{1}{g_{c1}^3}\right) \\[2mm]
b_{y\theta_z} &= b_a\ell\left(-\frac{1}{g_{a1}^3} + \frac{1}{g_{a2}^3} + \frac{1}{g_{a4}^3} - \frac{1}{g_{a5}^3}\right) \\[2mm]
b_{zz} &= b_a\left(\frac{1}{g_{a7}^3} + \frac{1}{g_{a8}^3} + \frac{1}{g_{a9}^3} + \frac{1}{g_{a10}^3} + \frac{1}{g_{a11}^3} + \frac{1}{g_{a12}^3}\right) + b_c\left(\frac{1}{g_{c4}^3} + \frac{1}{g_{c5}^3} + \frac{1}{g_{c6}^3}\right) \\[2mm]
b_{z\theta_x} &= \frac{b_a\ell\sqrt{3}}{2}\left(\frac{1}{g_{a7}^3} - \frac{1}{g_{a8}^3} + \frac{1}{g_{a10}^3} - \frac{1}{g_{a11}^3}\right) + \frac{b_c\ell\sqrt{3}}{2}\left(-\frac{1}{g_{c4}^3} + \frac{1}{g_{c5}^3}\right) \\[2mm]
b_{z\theta_y} &= \frac{b_a\ell}{2}\left(-\frac{1}{g_{a7}^3} - \frac{1}{g_{a8}^3} + \frac{2}{g_{a9}^3} - \frac{1}{g_{a10}^3} - \frac{1}{g_{a11}^3} + \frac{2}{g_{a12}^3}\right) + \frac{b_c\ell}{2}\left(\frac{1}{g_{c4}^3} + \frac{1}{g_{c5}^3} - \frac{2}{g_{c6}^3}\right) \\[2mm]
b_{\theta_x z} &= \frac{b_a\ell\sqrt{3}}{2}\left(\frac{1}{g_{a7}^3} - \frac{1}{g_{a8}^3} + \frac{1}{g_{a10}^3} - \frac{1}{g_{a11}^3}\right) + \frac{b_c\ell\sqrt{3}}{2}\left(-\frac{1}{g_{c4}^3} + \frac{1}{g_{c5}^3}\right) \\[2mm]
b_{\theta_x\theta_x} &= \frac{3b_a\ell^2}{4}\left(\frac{1}{g_{a7}^3} + \frac{1}{g_{a8}^3} + \frac{1}{g_{a10}^3} + \frac{1}{g_{a11}^3}\right) + \frac{3b_c\ell^2}{4}\left(\frac{1}{g_{c4}^3} + \frac{1}{g_{c5}^3}\right)
\end{aligned}
$$

$$b_{\theta_x\theta_y} = \frac{b_a\ell^2\sqrt{3}}{4}\left(-\frac{1}{g_{a7}^3}+\frac{1}{g_{a8}^3}-\frac{1}{g_{a10}^3}+\frac{1}{g_{a11}^3}\right)+\frac{b_c\ell^2\sqrt{3}}{4}\left(-\frac{1}{g_{c4}^3}+\frac{1}{g_{c5}^3}\right)$$

$$b_{\theta_yz} = \frac{b_a\ell}{2}\left(-\frac{1}{g_{a7}^3}-\frac{1}{g_{a8}^3}+\frac{2}{g_{a9}^3}-\frac{1}{g_{a10}^3}-\frac{1}{g_{a11}^3}+\frac{2}{g_{a12}^3}\right)+\frac{b_c\ell}{2}\left(\frac{1}{g_{c4}^3}+\frac{1}{g_{c5}^3}-\frac{2}{g_{c6}^3}\right)$$

$$b_{\theta_y\theta_x} = \frac{b_a\ell^2\sqrt{3}}{4}\left(-\frac{1}{g_{a7}^3}+\frac{1}{g_{a8}^3}-\frac{1}{g_{a10}^3}+\frac{1}{g_{a11}^3}\right)+\frac{b_c\ell^2\sqrt{3}}{4}\left(-\frac{1}{g_{c4}^3}+\frac{1}{g_{c5}^3}\right)$$

$$b_{\theta_y\theta_y} = \frac{b_a\ell^2}{4}\left(\frac{1}{g_{a7}^3}+\frac{1}{g_{a8}^3}+\frac{2}{g_{a9}^3}+\frac{1}{g_{a10}^3}+\frac{1}{g_{a11}^3}+\frac{2}{g_{a12}^3}\right)+\frac{b_c\ell^2}{4}\left(\frac{1}{g_{c4}^3}+\frac{1}{g_{c5}^3}+\frac{2}{g_{c6}^3}\right)$$

$$b_{\theta_zx} = b_c\ell\left(-\frac{1}{g_{c2}^3}+\frac{1}{g_{c3}^3}\right)$$

$$b_{\theta_zy} = b_a\ell\left(-\frac{1}{g_{a1}^3}+\frac{1}{g_{a2}^3}-\frac{1}{g_{a4}^3}+\frac{1}{g_{a5}^3}\right)$$

$$b_{\theta_z\theta_z} = b_a\ell^2\left(\frac{1}{g_{a1}^3}+\frac{1}{g_{a2}^3}+\frac{1}{g_{a4}^3}+\frac{1}{g_{a5}^3}\right)+b_c\ell^2\left(\frac{1}{g_{c2}^3}+\frac{1}{g_{c3}^3}\right)$$

The entire damping model can be describe more compactly through a matrix representation where $\mathbf{F} = \mathbf{BV}$ and $\mathbf{B}$ is defined as

$$\mathbf{B} = \begin{bmatrix} b_{xx} & 0 & 0 & 0 & 0 & b_{x\theta_z} \\ 0 & b_{yy} & 0 & 0 & 0 & b_{y\theta_z} \\ 0 & 0 & b_{zz} & b_{z\theta_x} & b_{z\theta_y} & 0 \\ 0 & 0 & b_{\theta_xz} & b_{\theta_x\theta_x} & b_{\theta_x\theta_y} & 0 \\ 0 & 0 & b_{\theta_yz} & b_{\theta_y\theta_x} & b_{\theta_y\theta_y} & 0 \\ b_{\theta_zx} & b_{\theta_zy} & 0 & 0 & 0 & b_{\theta_z\theta_z} \end{bmatrix}.$$